Title

Adaptive cortical processing of unattended sounds: neurocomputational underpinnings revealed by simultaneous EEG-MEG

Authors

Françoise Lecaignard[1,2,3] , Olivier Bertrand[1,2], Anne Caclin[1,2], Jérémie Mattout[1,2]

Affiliations

[1] Lyon Neuroscience Research Center, CRNL; INSERM, U1028; CNRS, UMR5292;

Brain Dynamics and Cognition Team, Lyon, F-69000, France

[2] University Lyon 1, Lyon, F-69000, France

[3] CERMEP Imaging Center, Lyon, F-69500, France

Corresponding author

Françoise Lecaignard, francoise.lecaignard@inserm.fr

Contact Information

Françoise Lecaignard

INSERM U1028 - CNRS UMR5292

Centre de Recherche en Neurosciences de Lyon

Equipe DYCOG

Centre Hospitalier Le Vinatier (Bât. 452)

95, Boulevard Pinel

69500 Bron, France

francoise.lecaignard@inserm.fr

Telephone: 0033 472138924

Fax: 0033 472138901

Abstract

Perceptual processes are shaped by past sensory experiences, raising the question of contextual adaptation of information processing in the brain. In predictive coding, the tuning of precision weights (PW) applying to sensory prediction errors (PE) enables such adaptation. We test this hypothesis with an original auditory oddball design to recover the respective neurophysiological encoding of PW and PE. Predictability of sound sequences was manipulated without the participants' knowledge to influence each quantity differentially. Using highly-informed EEG-MEG, trial-to-trial learning models were employed together with dynamic causal models (DCM) of deviance responses. Modelling results revealed Bayesian learning within a fronto-temporal network. Essentially, we show an automatic adaptation of learning and underlying connectivity to the contextual informational content. Predictability yielded a more informed learning with larger PW and lower PE, signaled by a decreased neuronal self-inhibition, and a decreased forward connectivity, respectively. These findings strongly support the predictive coding account of perception with automatic contextual adaptation.

Introduction

Recent computational theories describe the brain as a predictive agent in continuous interaction with its environment[1,2]. This view implies that every information (be it an internal belief or an incoming sensation) is processed probabilistically: the brain would estimate the confidence or precision it assigns to any information *in the current context of processing* [3]. In order to predict future sensations and adapt to environmental changes, the brain would constantly infer the context-dependent relative precision gain of prior beliefs and sensory information, termed as precision weight (PW). This dynamical process corresponds to the learning about the regularities present in the environment, referred to as *perceptual learning* [4,5].

These theoretical views of the brain have already succeeded in providing new and testable hypotheses, leading to new or revisited experimental paradigms to address how the brain adapts under uncertainty [6-10]. A striking example is the growing interest in how stimulus predictability modulates some long-established sensory responses [11-13]. However, beyond the great insights that those theories have already provided, the precise mental processes and neurophysiological mechanisms that subsume perceptual learning remain elusive. To date, no direct evidence of context-dependent precision weighting calculation and associated neuronal implementation has been reported. In this study, we sought to shed light on this important question by considering a simple form of perceptual learning, that could be at play during unattentional (passive) listening of sound sequences. We addressed the effect of the contextual relevance of information (if it was to be learnt implicitly by the brain) on auditory processing, using physiological and psychological dynamical modelling fitted to simultaneous EEG-MEG data.

The view of perception as a probabilistic inference has been augmented with predictive coding as a possible cognitive framework and a plausible neuronal implementation [14-17]. Contextual adaptation in predictive coding is driven by hierarchical *precision-weighted prediction errors* (PWPEs) induced by every incoming sensation [18]. Sensory PWPEs are computed at the lower level of the hierarchy as the combination of 1) a prediction error (PE) quantifying the unexpectedness of the current event, and 2) a precision weight (PW) balancing the expected reliability of the current sensation relative to the estimated reliability of internal predictions. Such context-sensitive PW enables to filter out errors that are irrelevant and, conversely, to gate errors that are relevant for optimal belief updating achieved higher in the hierarchy. This endows the brain with efficient and flexible perceptual processing. Beside, recent and influential advances in computational psychiatry [19,20] have led to a growing interest for the PW account in sensory processing as related dysfunctions could to be at the heart of psychopathology [21]. Hence, testing its neural account deserves serious consideration. So far, few but very encouraging results from trial-by-trial analysis of neuroimaging data have started addressing the computation of hierarchical PWPEs in a visual cue-association learning task [22] or an auditory detection task [23,24]. Here, we expand such studies by addressing the distinct neural representations of sensory PE and contextually adaptive PW.

To overcome the challenge to separate these quantities having interdependent dynamics [3] , we used:

- an experimental manipulation of the informational content of the environment, to induce distinguishable PE and PW contextual adjustments (see below)

- cognitive modelling of sound processing in the different informative contexts, to test perceptual learning - with related PE and PW - and its computational adaptation to the context
- neural models of underlying connectivity, to investigate the implementation of perceptual learning and the contextual effect on specific connection strengths theoretically assigned to PE and PW [4].

Precisely, we used an original version of the well-known oddball paradigm in order to elicit deviance responses [25] in different contexts of information relevance induced by the manipulation of deviant occurrence predictability. Predictable oddball tones are more expected and also more informative than unpredictable ones because they carry a structural (contextual) information in addition to obeying the oddball rule *per se*. As such, they generate smaller surprises hence reduced PEs, and these errors are themselves more informative, thereby signaled with a larger PW. To test these adaptive computations, we assumed the view of observable evoked responses (ERs) reflecting PWPEs [26], that is supported by modelling neuroimaging data at both the cognitive [23,24] and neurophysiological [27,28] levels. We conducted simultaneous EEG and MEG recordings [29] with the aim to reveal subtle changes of brain activity induced by the contextual manipulation. Examining classic deviance-related ERs during this paradigm evidenced brain's ability to learn automatically different contexts (predictable and unpredictable) [30]. Here we examine how such contextual learning computationally and physiologically modulates sound processing, leading to the reported ER modulations. Specifically, the modelling of typical deviance processing could evidence Bayesian perceptual learning (optimization of PE and PW) within a fronto-temporal network. Moreover, and critically, the predictability manipulation successfully exhibited changes in learning models at the cognitive level. Our findings reveal a larger time-

window of integration of information in perceptual learning under a structured environment. The physiological counterpart of such implicit tuning of learning could also be measured in the synaptic connectivity established by deviance processing. Precisely, we observed a decrease in self-inhibition within cortical areas (coding for a larger PW) together with a decrease in forward connectivity between cortical areas (coding for reduced PE or PWPE) with predictability. The fact that such combination of neuro- and computational modelling succeeded in providing a comprehensive description of the hypothesized contextually adaptive learning nicely illustrates the clear utility of influential David Marr's framework in studying and understanding brain information processing [31] .

Results

We report findings from simultaneous EEG-MEG recordings in 20 healthy volunteers undergoing a passive auditory oddball paradigm in two contexts of predictability: frequency deviants were delivered either within a purely deterministic context (condition PC, predictable context), or a pseudo-random one (condition UC, unpredictable context) (Figure 1). The results presented here were obtained from a four-step modelling procedure. Its ultimate goal was to test the existence of implicit perceptual learning during passive listening and, where appropriate, to disclose the neurophysiological signature of PE and PW computation made distinct by the predictability manipulation. Trial-by-trial computational modelling and dynamic causal models (DCM) of averaged responses [32] were applied to characterize perceptual learning at the cognitive and neurophysiological levels, respectively. First analysis aimed at testing the hypothesis of perceptual learning (vs. no-learning scenarios) at play during oddball sound processing using computational models (*PL-oddball* analysis, conditions UC and PC). Secondly, using DCM, we addressed the cortical implementation of this learning process (*DCM-oddball* analysis, UC and PC). In a third step, we tested whether the brain adapts its learning style to the contextual manipulation (*PL-predictability* analysis, PC vs. UC). The latter provided clear predictions regarding the mapping of PE and PW onto physiology, which we tested in a final step, using Dynamic Causal Modelling (*DCM-predictability* analysis, PC vs. UC).

The implicit learning of the two different statistical structures was demonstrated in a previous report [30]: at the EEG sensor level a significant reduction of mismatch responses (at different latencies) was observed under predictability while none of the participants reported having noticed our contextual manipulation. In the present study,

computational learning models were fitted to single-trial data whereas DCM analysis rested on the simultaneous inversion of standard (preceding a deviant) and deviant ERs (see Methods).

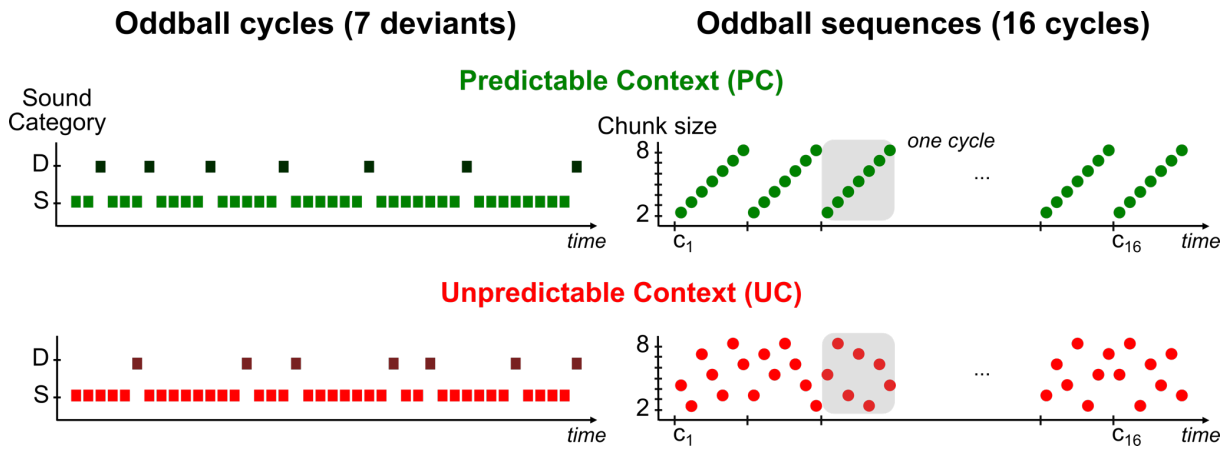

Figure 1. Experimental Design. *Left, Schematic view of typical oddball cycles in the predictable (green, top) and unpredictable (red, bottom) contexts. Both cycles correspond to the same deviant probability (p = 1/6). They only differ in the transition between segments of repeating standards (chunks), which are sorted by increasing size in condition PC. Right, Representation of oddball sequences as a function of chunk size reveals the different statistical structures applying on the same oddball rule in context PC (green, top) and UC (red, bottom). X-axis ticks indicate the beginning of each cycle (sequences comprised 16 cycles, c_1 to c_{16}). Grey rectangles delineate the exemplary cycle depicted on the left for both sequences. S: Standard, D: Deviant.*

Perceptual learning of environmental regularities (*PL-oddball* analysis)

Under predictive coding mismatch responses (including the Mismatch Negativity, MMN) elicited by unexpected deviants reflect prediction errors of a continuously updated model of the acoustic environment [26]. We tested this hypothesis against alternative cognitive processes that did not involve perceptual learning (presented below), and corresponding models were all defined as a two-level linear model of the form:

$$\begin{cases} y = X\theta_1 + \theta_2 + \varepsilon_1 \\ \theta_1 = 0 + \varepsilon_2 \\ \theta_2 = 0 + \varepsilon_3 \end{cases} \quad (1)$$

Where y indicates the reconstructed cortical activity informed by a fused EEG-MEG source inversion [33] in the form of a vector of trial-by-trial activity at a particular sample of the peristimulus time; X is defined for each model and represents the predicted trajectory of PWPE over the sound sequence; $\{\theta_1, \theta_2\}$ and $\{\varepsilon_1, \varepsilon_2, \varepsilon_3\}$ refer to Gaussian observation parameters and Gaussian noise, respectively. Vector y was defined for each time sample of the [-50 +350] ms epoch and for each cluster of the MMN cortical network identified at the group level. Three clusters were found in each hemisphere, in the Heschl's Gyrus (HG), the Planum Polare (PP) and the Inferior Frontal Gyrus (IFG) (Figure 2.A). We considered a model space of seven cognitive models partitioned into three families, largely inspired by models used in a previous tactile oddball study [23]:

- Family fam_{null} is made of a single model, the null model (M0) assuming that the brain response to every tone is the same, or equivalently that EEG fluctuations only reflect random noise (i.e. $\theta_1 = 0$ in Eq.1).
- Family fam_{noL} contains two non-learning or static models, namely "change detection" (CD) and "linear change detection" (LinCD). Both assume that the brain simply compares each incoming sensation to the preceding one. In model CD, X_k at trial k is assigned to 0 if the kth stimulus is equal to the preceding one, and 1 otherwise. Model LinDC is similar to CD but assigns a prediction error proportional to the number of preceding sounds that differ from the one being currently observed [23,24].
- Family fam_L includes Bayesian perceptual learning models assuming that the

brain estimates the probability μ to hear a standard (under a Bernoulli distribution, see Methods). These models involve a temporal integration window that allows down-weighting the influence of past events and whose size is defined by a time constant parameter (τ). We considered four different values for τ (2, 6, 10 and 100), leading to four models in fam_L. PWPE computed at each trial quantifies the belief update about μ and was defined as the Bayesian Surprise (BS; the Kullback-Leibler divergence between the prior and the posterior distribution of μ, see Methods). The BS, hence PWPE, decreases with τ, as can be seen in Supplementary Figure 1.

These models were all fitted to the reconstructed cortical activity in both PC and UC conditions. For each source and at each time sample of the peristimulus interval, model inversions were performed following a meta-Bayesian approach using the VBA toolbox [34] and model families were compared to each other using an RFX family-level inference [35]. As shown in Figure 2.B, the Null hypothesis (fam_{null}) was found to outperform the other families, at every time sample and every cortical source, except for the time interval of the MMN. Precisely, posterior exceedance probability of family fam_L was found to be significantly greater than the ones of the other families between 150 ms and 200 ms (6 samples), in the left and right Heschl's Gyrus (HG), between 130 ms and 180 ms (6 samples) and at 150 ms (1 sample) in the left and right Planum Polare (PP), respectively, and between 130 ms and 200 ms (8 samples) and between 140 ms and 190 ms (6 samples) in the left and right Inferior Frontal Gyrus (IFG), respectively. Noticeably, in the latency range of the P3a described in Lecaignard et al.[30], the Null hypothesis could also be challenged by learning models, as suggested by the increase of fam_L posterior exceedance probability, an effect most visible in left IFG.

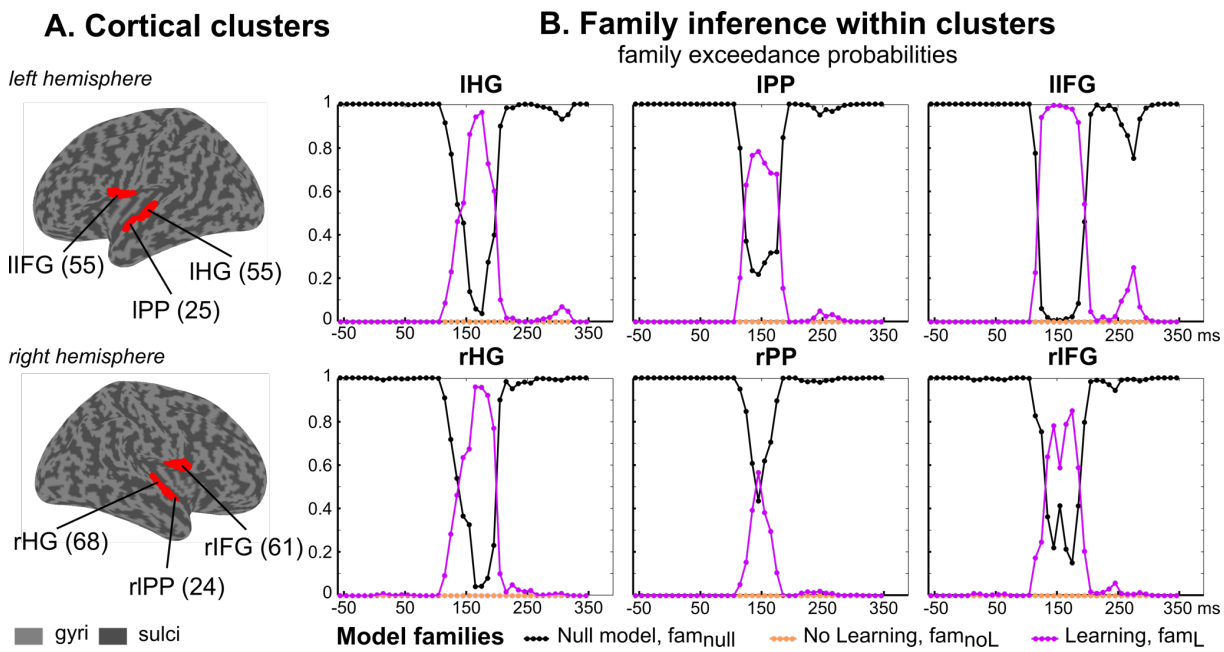

Figure 2. Computational modelling of deviance processing. *A) Cortical clusters involved in* PL-oddball *modelling are represented (red) over the inflated cortical surface of the SPM template brain* [36]*. These six clusters are left, right Heschl's Gyrus (lHG, rHG), left, right Planum Polare (lPP, rPP) and left, right Inferior Frontal Gyrus (lIFG, rIFG). Total number of nodes in each cluster is indicated in parenthesis (see also Supplementary Figure 2.B). Within each cluster, reconstructed single-trial traces (informed by EEG and MEG) were averaged over nodes and confronted to trial-by-trial model predictions (for every model of* PL-oddball *model space) at each time sample within [-50 +350] ms. B) Family-wise Bayesian model comparison. For each cluster and at each time sample, family inference provides the estimated posterior family exceedance probability of each model family (fam_{null}: black, fam_{noL}: orange, fam_L: pink).*

Perceptual learning in a four-level fronto-temporal network (*DCM-oddball* analysis)

The previous analysis reveals implicit perceptual learning of acoustic regularities during an oddball sequence, at the latency of the MMN. Following a predictive coding view, perceptual learning implies PWPE computations in the brain. From this, the question naturally arises as to what are the corresponding underlying neurophysiological mechanisms. We test the hypothesis that PWPEs are conveyed

upwards in the cortical hierarchy through feedforward connections, and trigger descending prediction messages using DCM. DCMs for evoked responses rely on a mesoscopic model of the cortical laminar circuitry (*Canonical Micro-Circuit*, CMC, see Supplementary Figure 3) which enables testing formally the mapping of computational learning quantities onto cortical representations [17,28]. Inspired by previous DCMs of the MMN [27,37], and guided by current learning model predictions, we addressed the two following questions: what is the structure of the network engaged in typical oddball sequence processing? Within this auditory network, what modulation of effective connectivity supports deviant compared to standard tone processing? This analysis combines in a Bayesian way posterior DCMs inferred separately in conditions UC and PC, using EEG and MEG signals (see Method).

Network characterization. We start by characterizing network architecture and input. Regarding the former, most reports of the DCM of the MMN entailed a three-level hierarchy [10,38-41]. However, the complementary EEG and MEG topographical information regarding the predictability modulation of the MMN peak led us to test an additional level. Indeed, this predictability effect was larger at fronto-central sites in EEG [30] and at temporal gradiometers in MEG (Supplementary Figure 2.A), in a way that suggests superior frontal generators expressing poorly on frontal gradiometers. We could identify bilateral clusters of activity in this region, with however limited precision (see Methods). The resulting four-level DCM structure was composed of eight sources distributed bilaterally over (from the lowest to the highest level) HG, PP, IFG and a superior frontal area SF (Figure 3.A). We connected these sources with intra-hemispherical bidirectional (forward and backward) connections. Alternative hypotheses entailed two- and three-level networks allowing to test the hierarchical depth as well as the contribution of PP and SF sources, leading to five model families

(*A1*, *A2*, *A3*, *A4* and *A5;* see Methods). Regarding DCM inputs, all models included a direct input to bilateral HG. In addition, inputs targeting IFG sources (known to receive direct thalamic afferents) were tested as the source-reconstructed EEG and MEG evoked responses suggested that frontal regions were activated prior to temporal ones (echoing a still-debated issue in the MMN literature)[42]. The input factor thereby included two levels (*HG* and *HG-IFG*). Considering the integration over different forms of standard-to-deviant modulations of connectivity, the resulting model space comprised a total of 36 DCMs (for a full description see Methods, *Network-Structure* model space). Each model inversion was performed on standard (just preceding the deviant) and deviant ERs, in condition UC and PC and for EEG and MEG data separately (leading to four inversions per subject and per model). Resulting explained variance averaged across models and subjects was equal 92.5% (standard deviation: ±10.5) and 78.1% (±11.6) in EEG and MEG, respectively (condition UC), and to 91.9% (±12.1) and 78.1% (±11.6) in EEG and MEG, resp. (condition PC). Posterior fusion of EEG and MEG DCMs (denoted p-MEEG) was achieved by applying Bayes' rule (see Methods). In the p-MEEG modality, family level inference revealed that family *A5* outperformed other model families with a posterior confidence probability (*pcp*) and posterior exceedance probability (*pep*) of 0.68 and >0.99, respectively (Figure 3.B). Regarding the DCM inputs (Figure 3.C), family level inference was clearly in favor of models with inputs arriving in both HG and IFG sources (*pcp* / *pep*: 0.82 / >0.99).

Deviance-related changes in connectivity.

Considering the winning DCM structure (architecture *A5* with four levels of hierarchy and input *HG-IFG*), we next examined the extrinsic and the intrinsic connectivity that govern the neural coupling between and within cortical sources, respectively. We

defined every extrinsic and intrinsic connection strength to account for standard processing and tested which connection strengths were modulated using a trial-specific gain accounting for deviant-related changes (Trial-specific modulation, TSM). The present analysis rests on a model space composed of 14 models (*Coupling-Change* model space, see Methods) designed to especially address TSMs. Explained variance was equal to (results for condition UC / condition PC): 96.5% (±5.1) / 97.8% (±2.7), for EEG, and 87.1% (±7.4) / 87.5% (±5.5) for MEG. We found evidence for forward, backward and intrinsic TSMs (*pcp* / *pep*: 0.82 / >0.99; 0.73 / 0.99; 0.73 / 0.99, resp.) in line with pioneering DCMs of the MMN [37,38]. In order to further characterize the deviant-related direction of change, we examined group-level posterior estimates of TSM obtained with Bayesian model averaging (BMA) over model space and subjects (see Methods). Over the entire network and in both conditions, we found standard-to-deviant modulations that fits well with predictive coding message-passing expectations. In particular, we found larger forward coupling for deviants (Figure 3.D; average and standard error across the network of group-level BMA estimates of forward TSM. UC: 1.145 ± 0.057, present in 5 out of 6 forward connections; PC: 1.027 ± 0.042, 4 out of 6 connections). We also found the expected increase of backward TSM (UC: 1.179 ± 0.073, 5 out of 6 connections; PC: 1.307 ± 0.112, 5 out of 6 connections) and a decrease of the intrinsic TSM (UC: 0.947 ± 0.064, 5 out of 8 connections. PC: 0.956 ± 0.047, 5 out of 8 connections).

Taken together, *DCM-oddball* findings support the neural implementation of predictive coding message passing along the cortical auditory hierarchy. These findings are in particular compatible with forward connections conveying ascending PWPEs being larger for unexpected deviant stimuli (Supplementary Figure 1). One of the great relevance of DCM with CMC for this work is that the micro-circuitry within each source

formally models predictive coding: it assigns in particular a prediction error unit to the superficial pyramidal (SP) cells, and accounts for the precision weighting of PEs by means of a self-inhibition parameter governing the excitability of subpopulation SP [17,43]. The reduced self-inhibition in subpopulation SP observed with deviants (which derives from the above-reported reduced intrinsic TSM, and is equivalent to a larger excitability in the supposed error units) could reflect a larger PW when processing unexpected inputs. However, it could alternatively encode the larger PWPE evidenced with deviants just like the forward connectivity (this would counter the theoretical neural representation of PW). To resolve such ambiguous mapping, we next consider the contextual predictability manipulation, that should influence differentially forward and SP self-inhibition connectivity if these were to encode PE (or PWPE) and PW respectively. Of course, testing this hypothesis requires to first evidence the adaption of perceptual learning to predictability.

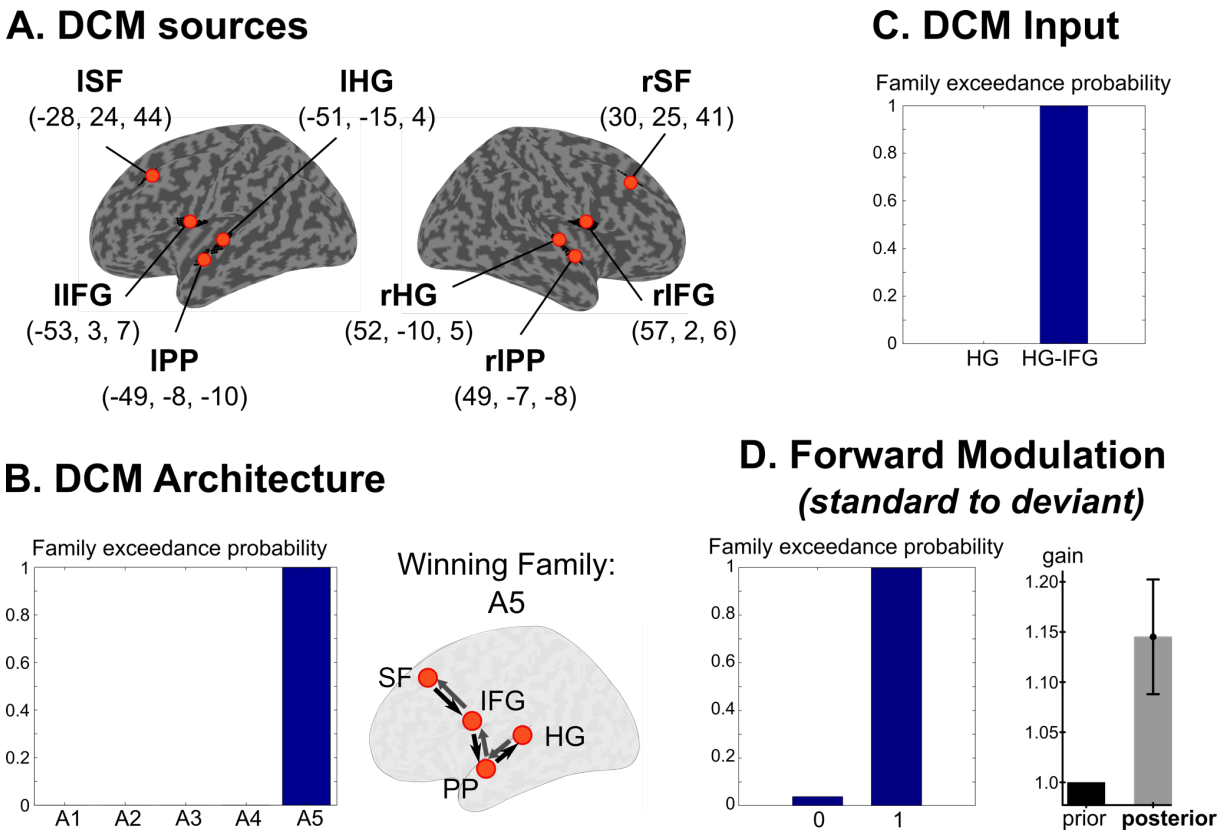

Figure 3. Dynamic causal modelling of deviance processing, using p-MEEG. *A) Cortical sources for DCM analysis. Each source is indicated schematically with orange dots on the inflated cortex (SPM template brain), with corresponding MNI coordinates (mm) in parenthesis. B) Family inference for DCM architecture: family exceedance probabilities (left) and corresponding network for the winning family A5 (right) following the notations and color codes of Supplementary Figure 3. C) Family inference for DCM inputs (family exceedance probabilities). D) Family inference for standard-to-deviant trial-specific modulation (TSM) for the forward connectivity. Family exceedance probabilities of the model families with disabled (0) and enabled TSM (1) is provided (left) and group-level BMA estimates of TSM values (in condition UC) averaged over the DCM network is represented (right). Prior value of TSM (black bar) was set to 1 assuming no standard-to-deviant modulation. Labels for the cortical sources and model families are provided in the main text.*

Contextual adaptation of perceptual learning (*PL-predictability* analysis)

Following the reasoning above, we tested in a third step whether the brain adapts its learning style to the contextual manipulation (*PL-predictability* analysis, PC vs. UC). We compared conditions PC and UC varying the informational value carried by similar stimuli, hence influencing sensory PE and PW differently. Precisely, the deterministic structure of sound sequence in condition PC emerges from specific transitions between sounds that have been added to the oddball rule in condition UC. Since such transition rules can be learnt within a predictive coding framework, better predictions regarding incoming sounds are achieved as predictability increases. This is equivalent to lower sensory PE with predictability. Besides, from an information theory perspective, sensory prediction errors in condition PC have a greater relevance for an optimal learning due to the fact that every sound in a predictable environment conveys more information than when delivered in an unpredictable one. Such larger relevance can be signaled as such with larger PW. In other words, predictability yields smaller but more relevant PE, hence lower PE and larger PW. Passive listening was used to

avoid presumable confounding effects of voluntary attention on PW [44]. The implicit learning process was already evidenced from the modulation of mismatch responses observed at the sensor-level on averaged ERPs [30].

As briefly mentioned in *PL-oddball* analysis, we introduced a temporal integration window in fam_L models as proposed by Ostwald et al. [23], whose size is an increasing function of τ (see Methods). Crucially, beyond the memory-based interpretation (the brain may arguably not be able to deal with long-gone, past information), this parameter endows the learning models with a flexible way to integrate past information and formalizes brain adaptation to its environment. Precisely, the above-mentioned decrease of Bayesian Surprise (BS) with τ (Supplementary Figure 1) and the reduced mismatch responses measured in the predictable context led us to expect that passive sound processing under context PC would rest on a larger temporal integration window (larger τ) compared to the one under context UC. Prior to testing this prediction, we simulated the grand-averaged MMN amplitude for each condition and different values of τ (the MMN was computed as the difference of the average BS measured for deviants and for standards preceding a deviant; see Methods). Results show that the (simulated) MMN amplitude decreases as τ increases. Interestingly, they also show a similar amplitude across contexts, for a given τ value (Figure 4.A). This suggests that the sequence alone cannot explain the MMN reduction in condition PC and a reduced τ under a more predictable sequence (demonstrating an adaptive learning) is thus expected in order to explain the observed sensor-level difference in ERs between UC and PC [30]. Using EEG-MEG reconstructed cortical data, we performed model inversion separately for condition PC and UC, at every time sample exhibiting statistical significance in the *PL-oddball* analysis. Crucially, τ was no longer fixed here but estimated. For each source and each parameter, posterior estimates were averaged

across samples; they were subsequently compared by a repeated-measures ANOVA across factors *Condition* (UC, PC), *Hemisphere* (Left, Right) and *Sources* (HG, PP, IFG). Larger τ values were found with condition PC compared to condition UC ($F_{(1,19)} = 10.13$; $p = 0.002$). On average across sources, τ was equal to 16.0 and to 21.3 with UC and PC, respectively (Figure 4.B). The ANOVA showed no other significant effect (all $p>0.12$). As can be seen in Figure 4.C, the different τ values in UC and PC generate different down-weightings of past observations, with a larger amount of information integrated during perceptual learning in the predictable context.

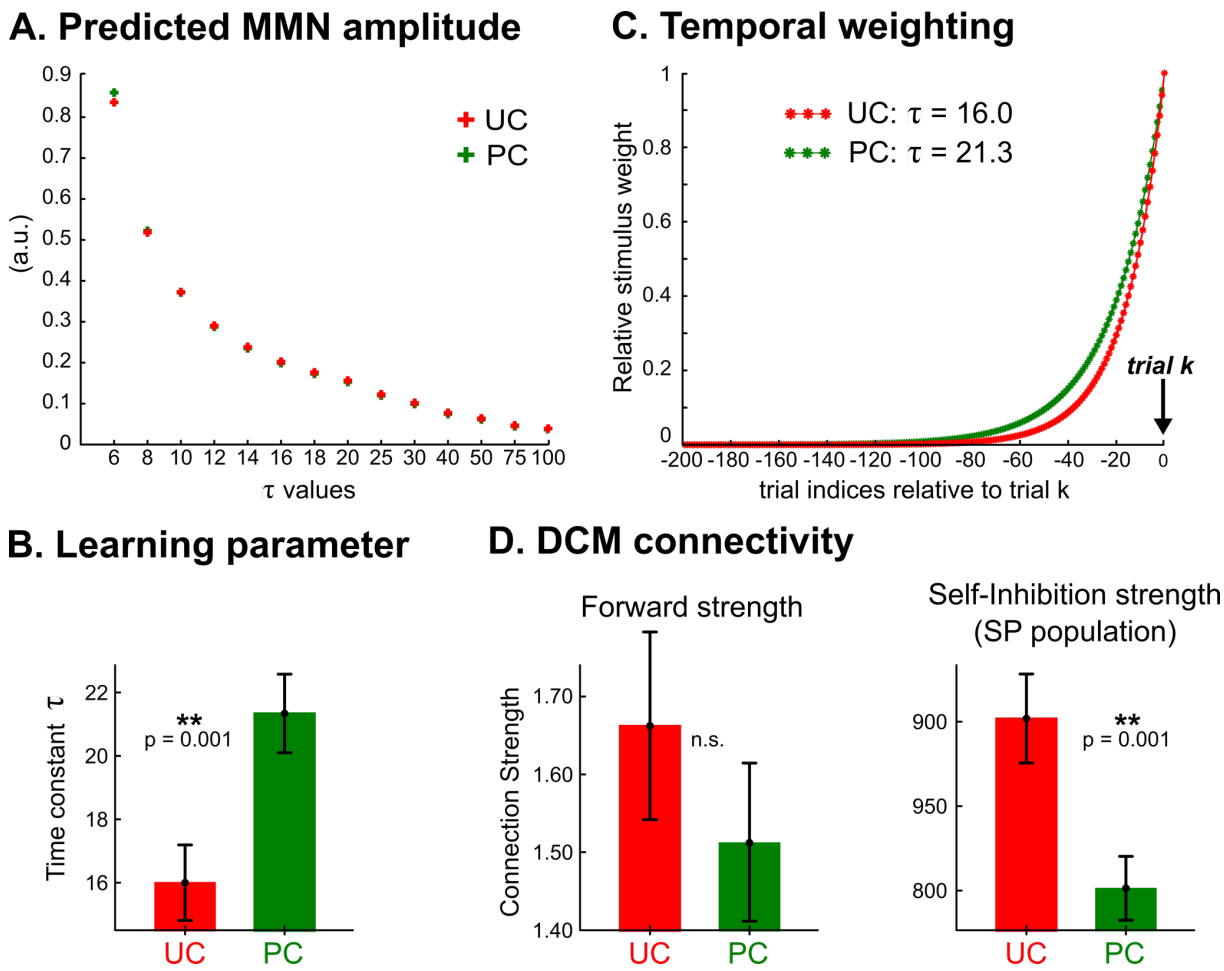

Figure 4. Effect of predictability on auditory processing. *Panels A, B and C refer to the cognitive modelling of the contextual manipulation (PL-predictability), and panel D to its physiological counterpart (DCM-predictability). A) Learning model predictions of the MMN amplitude (group average) as a function of τ for UC (red) and PC (green)*

sound sequences (see Methods). Note that in both contexts, MMN amplitude decreases similarly as τ increases. B) Effect of predictability on learning parameter τ. Posterior estimates of τ averaged at the group-level and over the six clusters exhibited a significant difference between conditions. C) Downweighting of past observations obtained with the posterior estimates of τ for conditions UC (red) and PC (green), respectively. D) Effect of predictability onto effective connectivity, using p-MEEG. Posterior estimates of forward (left) and self-inhibition (right) strengths measured in both conditions (UC: red, PC: green); averaged over the group and over the connections within the (DCM) network. SP: superficial pyramidal; a. u.: arbitrary units.

Separate neural correlates of PE and PW (*DCM-predictability* analysis)

Perceptual learning was shown to adapt automatically to predictability. We finally examined whether predictability also shapes the effective connectivity at play during deviance processing, with the aim of clarifying the neural representation of key learning quantities (PE, PW). This analysis rests on individual BMA posterior estimates of DCM parameters (in the p-MEEG modality) computed in both conditions separately. Findings from the *PL-predictability* analysis provided explicit hypotheses regarding the effect of predictability on the extrinsic forward and intrinsic self-inhibition connections [17,26]. Namely, we expected:

1) Lower forward connection strength in condition PC, if it was to encode PE or PWPE.
2) Lower SP self-inhibition connection strength (hence larger SP excitability) in condition PC, if it was to encode PW.

To test first prediction, we conducted a repeated-measures ANOVA over forward connection strength estimates, with factors *Condition* (UC, PC), *Hemisphere* (Left, Right) and *Level* (HG-PP, PP-IFG, IFG-SF). As can be seen in Figure 4.D (left), predictability yielded a reduced forward connection strength on average across the network (average with standard error: 1.51 ± 0.10 and 1.66 ± 0.12, in PC and UC resp.),

an effect which was largest at the lowest level of the network (PC / UC. Level HG-PP: 1.52 ± 0.10 / 2.05 ± 0.24; Level PP-IFG: 1.41 ± 0.16 / 1.50 ± 0.21; Level IFG-SF: 1.61 ± 0.24 / 1.44 ± 0.17). However, these effects did not reach statistical significance (*Condition*: $F_{(1,19)}$=0.84; p=0.36; *Condition*×*Level*: $F_{(1,19)}$=1.82; p=0.17). The second prediction was further tested with a similar ANOVA over BMA self-inhibition estimates, here factor *Level* comprised four levels (HG, PP, IFG, SF). There was a significantly reduced self-inhibition connection strength in population SP in condition PC compared to condition UC (801.4 ± 18.9 and 901.9 ± 26.3, resp.; $F_{(1,19)}$ = 10.52; p = 0.001), as shown in Figure 4.D (right). This result establishes a link between self-inhibition in SP and PW, as both adapt consistently to predictability. Finally, the ANOVA was conducted on standard-to-deviant TSM applying on forward and intrinsic connections. We found no significant main effect of *Condition* (forward: $F_{(1,19)}$=2.50; p=0.12; intrinsic: $F_{(1,19)}$=0.01; p=0.90). These latter results suggest that the contextual effect of our predictability manipulation apply indistinctively to standard and deviant stimuli processing.

Discussion

This work addressed the hierarchical processing of sensory information during unattentional listening through its adaptation to the statistical structure of the environment. Complementary cognitive and neurophysiological modelling of oddball responses collected during different contexts of predictability reveals the occurrence of perceptual learning within a fronto-temporal hierarchy, as expected in the predictive coding framework. Moreover, it formally demonstrates that this predictive process is shaped by predictability in a way that optimizes the integration of relevant sensory information over time. Computationally speaking, this adaptation relies on the tuning of the precision weighting of prediction errors, a process which is known to be a cornerstone of Bayesian information processing [3]. We therefore show with a mechanistic and dynamical approach that during passive oddball listening, the more structured is the environment, the more efficient is sound processing. Besides, for the first time the neural encoding of precision weight could be distinguished from the prediction error *per se* and directly attributed to inhibitory mechanisms. Remarkably, the hypothesis of ERs reflecting hidden PWPEs [26] that was considered along this work is substantiated empirically by the present findings obtained with complementary neuro- and computational generative models of evoked responses.

Our report of perceptual learning evidenced at the MMN latency and deploying within a hierarchical fronto-temporal network fits very well with predictive processing of sensory information. Findings in the *LM*- and *DCM-oddball* analyses thus add to the rare but robust empirical supports for this theory in oddball processing, obtained with trial-by-trial computational modelling [23,24] and DCM [38]. Here, both levels of description could be addressed using exactly the same EEG-MEG datasets (rejected epochs were

identical across analyses and across modalities), ensuring that their respective findings, informed from the cortical reconstruction of single trials (*LM-oddball*) and evoked responses (*DCM-oddball*) reflect perfectly the same brain activity.

The major contribution of this work, in the perspective of testing predictive coding more finely, lies in the fact that we could evidence the automatic tuning of the precision weighting of sensory errors and relate it to inhibitory mechanisms. This was made possible with the proposed model-driven contextual manipulation, where a second-order rule applies on the first-order oddball one. At the cognitive level, *PL-predictability* analysis demonstrates quantitatively brain's ability to grasp implicitly the larger informational content of the predictable context to derive a more informed and more efficient learning at the sensory level (by means of a larger temporal integration window). The larger efficiency in sensory processing translates into more accurate sensory predictions and more rapid adaptation to unexpectedness (PW is related to the learning rate)[3]. This could provide a mechanistic explanation to the better task performances reported in target detection during the listening of regular auditory streams akin random ones [45], and also during the processing of words and music stimuli under contextual expectancy [46]. Similar facilitation of sensory processing in a structured environment was also suggested in a visual discrimination study [47], where temporal expectation was found to decrease reaction time, and could be associated to an increase of the sensory gain using a diffusion model. This result is comparable to the present PW adaptation, that here occurs without attentional (active) processing. At the neural level, our findings support the view of forward connections carrying PWPE computed in supragranular cortical layers, and establish empirically a direct link between PW and self-inhibition of subpopulation SP. Several recent DCM studies strongly supported this PW / self-inhibition mapping, as they reported consistent

modulations of SP self-inhibition by some experimental manipulations hypothesized to influence PW under predictive coding, namely a cholinergic neuromodulation [28], sensory precision [43], selective attention [48], and predictability [49]. Here, it is the automatic contextual adaptation of sensory processing that we reveal *computationally* and *physiologically* that fills the missing link enabling to relate PW and SP self-inhibition directly. From a methodological perspective, DCM findings add to recent efforts to increase model plausibility to account for electrophysiological data [50,51].

The present work contributes to better characterize the cortical hierarchy involved in auditory processing. There is a growing convergence of findings supporting hierarchical error processing within a fronto-temporal network, with consistency across various methodologies [25,30,52-55]. Regarding the structure of the cortical network, we provide findings in favor of a four-level structure during deviance processing, which has not been tested so far to our knowledge. The superior frontal upper level involves however cortical sources whose precise locations could not be assessed. Still, four-level models were clearly selected by family model inference, a result that emphasizes the need for such additional frontal contribution to account for the dynamics of oddball responses (an example of poorly spatially resolved source with great dynamic relevance can be found in David et al. [56]). Note that the study does not address the computational role of each DCM level. Rather we considered a single hierarchical-level learning based on a simple Bernoulli distribution (other, slightly more complex transition probability models could be considered, e.g. see Meyniel et al., [57]) because it was equipped to reveal an adaptive learning in combination with the contextual manipulation. Such adaptation requires hierarchical learning to emerge, as higher levels compute errors and related precisions that pertain to more stable or slow-changing (contextual) stimulus features [14]. In addition, increasing second-order

statistic reliability has been theoretically demonstrated to increase the precision-weighting of sensory errors [58,59]. The present report of automatic adaptation of perceptual learning and the related tuning of underlying connectivity fits very well with the top-down influence of contextual learning on sensory processing.

Future research in testing predictive brain theories for perception has to address the mechanisms which subsume the adaptation of the learning process that we observed, including the dynamics of PW tuning. From a network perspective, we believe that investigating the precise role of the IFG in perceptual learning would be a relevant strategy. Indeed, the related findings obtained at both levels of modelling appear indicative of the IFG being a key contributor in regularity learning. Precisely, the IFG exhibited bilaterally perceptual learning at the MMN latency (and to a lesser extent at the P3a latency in the left hemisphere), and was found to receive a direct sensory input in DCM, a result which is consistent with previous DCM reports by Phillips et al. [39,51]. Such early implication which further pursues in response to feedback messages from the superior frontal level indicates a major involvement of this region all along deviance processing resulting in the MMN at the sensor level (and the P3, [52]. Other studies have also identified this region as a key node in hierarchical auditory processing. Using trajectories of DCM SP self-inhibition during the listening of regular and random streams, the IFG was proposed to exert a backward influence onto the precision-weighting of lower-level predictions [49]. Another example shows the implication of the right inferior / middle frontal gyrus in hierarchical learning in an active probability learning task [60]. These promising findings encourage to further probe with our neuro-computational approach how Bayesian learning manifests in this region in particular. Targeting the IFG could be done using invasive electrocorticography or intracranial recordings (in epileptic patients) to take advantage of their high spatio-temporal

resolution. The use of continuously varying contextual relevance could help at better understanding the implication of the IFG in the dynamics of adaptive precision weighting (within the interplay of information flows).

In addition, and related to this, from a psychological perspective we aim at investigating more finely the present predictability adaptation in relation to attentional processes, guided by the computational account of attention [26]. Under this view, attention serves to collect contextually-informative sensations to optimize perception and learning [26,37,61], through either the precision weighting of sensory channels [44] or action. The view of attention as the tuning of PW echoes our findings obtained without participant's awareness of the experimental manipulation. Interestingly, predictive brain theories have led to consider under the same framework the opposite effect of voluntary attention (an increase) and predictability (a decrease) on ER amplitudes reflecting PWPEs. In Chennu et al. [53] and in Auksztulewicz and Friston [10], both factors could be manipulated orthogonally using different task instructions during perception of oddball-like sound sequences. These two studies revealed different modulations of mismatch responses at different latencies, and related attention to SP self-inhibition using DCM, respectively. Chennu and colleagues reported a reduced MMN when attention was explicitly engaged towards (local) tone transitions compared to (global) multi-tone patterns. This fits with the present reduced MMN in the predictable condition considering that a more informed learning of the oddball rule (providing better predictions) could be at play either through an explicit attentional engagement or, in our case, through the implicit learning of the contextual information. Therefore, we argue that likewise but without the voluntary orientation of attention, predictability acts as an implicit attentional process, enhancing the efficiency of sensory processing. Similar effect of voluntary attention and predictability on PW (an increase) emphasizes

the great potential of separating PE and PW accounts in order to predict (and test) their respective effects on ERs, instead of addressing PWPEs as a whole (for review, see Heilbron and Chait [12]). Bridging passive predictability processing and voluntary attention opens the way to mechanistically investigate attentional capture. This would involve experimental manipulations of PW and PE, and appropriate hierarchical dynamic models to assess underlying activity, and feasibility was demonstrated here. We expect in particular novel insights from the manipulation of PW (in addition to typical modulations of global PWPEs), to assess whether voluntary attention can emerge from specific PW evolution reflecting a form of evidence accumulation. Here again, the IFG could play a key role (in keeping with its acknowledge contribution to attentional processes and the P3a)[62].

Conclusion

An oddball paradigm was used to test regularity learning during auditory processing and predictability was further manipulated to disentangle PE and PW neural representations. Precisely, this contextual effect was found to increase the extent of temporal integration of past information, which implies lower sensory prediction errors amplified by a larger precision weighting. Findings in this paper 1) demonstrate the conclusive power of modelling approaches combining neuronal and cognitive levels and 2) emphasize the importance of accounting for the encoding of precision weighting when investigating perceptual learning and decision-making. Unfolding the mechanisms of precision tuning and encoding, especially at an implicit level, is a potentially critical step for clinical applications as alterations of these processes have been suggested to be at the core of several psychiatric disorders [19,21]. Applying such a simple oddball paradigm, only involving passive listening, coupled with computational and neurophysiological modelling could be of great value in this context.

Methods

Participants. Twenty healthy volunteers (10 female, mean age 25±5 years, ranging from 18 to 35) participated in the study. All participants were free from neurological or psychiatric disorder, and reported normal hearing. All participants gave written informed consent and were paid for their participation. Ethical approval was obtained from the appropriate regional ethics committee on Human Research (CPP Sud-Est IV - 2010-A00301-38).

Experimental design. Predictable and unpredictable sound sequences embedding a typical frequency oddball rule (conditions PC and UC, respectively) were used in the present study. Participants were instructed to ignore the sounds and watch a silent movie of their choice with subtitles. Predictable sound sequences comprised 16 cycles that were each made of a repeating 42-tone pattern following the deterministic incrementing rule depicted in Figure 1. Unpredictable sequences corresponded to pseudo-random oddball sequences typically used in oddball paradigms, with specific controls for the number of standards in between two deviants. Despite their differing statistical structure, both sequence types had the same deviant probability ($p = 0.17$) and the same distribution of deviants among standards (there were exactly the same number of chunks of repeating standards before a deviant in both conditions, with chunk size varying from 2 to 8 standards). Further details about stimuli and sequences can be found in Lecaignard et al. [30]. All stimuli were delivered using Presentation software (Neurobehavioral Systems, Albany, CA, USA).

Data acquisition and pre-processing. Simultaneous MEG and EEG recordings were carried out in a magnetically shielded room with a whole-head 275-channel

gradiometer (CTF-275 by VSM Medtech Inc.) and the CTF-supplied EEG recording system (63 electrodes), respectively. Signal was amplified, band-pass filtered (0.016–150 Hz), digitized (sampling frequency 600 Hz) and stored for off-line analysis. First-order spatial gradient noise cancellation was applied to MEG signal. EEG reference and ground electrodes were placed on the tip of the nose and left shoulder, respectively. Digitization of electrode locations (Fastrak, Polhemus, Colchester, VT, USA) and acquisition of individual T1-weighted magnetic resonance imaging images (MRIs, Magnetom Sonata 1.5 T, Siemens, Erlangen, Germany) were conducted for coregistration purposes in distributed source reconstruction (see below).

Pre-processing of data using the ELAN package [63] and Matlab routines included the following: rejection of data segments affected by head movements (larger than 15 mm relative to the average position over sessions) or SQUID jumps, power-line filtering (stop-band filters centered on 50 Hz, 100 Hz, and 150 Hz with bandwidth of ± 2 Hz), independent component analysis (ICA) correction for ocular artifacts (EEGlab routines, http://sccn.ucsd.edu/eeglab/index.html), rejection of trial epochs (from -200 ms to 410 ms after stimulus onset) with signal amplitude range (over entire epoch) exceeding 2000 fT for MEG data and 150 μV for EEG data, and 2-45 Hz band-pass digital filtering (bidirectional Butterworth, 4th order). Importantly, we only used time epochs that survived the procedures applied for artifact rejection for both modalities. Finally, trial epochs were imported in SPM (Wellcome Department of Imaging Neuroscience, http://www.fil.ion.ucl.ac.uk/spm) and were down-sampled (200 Hz) for data reduction and low-pass filtered (20 Hz low-pass digital filter, bidirectional Butterworth, 5th order). Group-average deviance responses obtained in EEG and MEG in both UC and PC conditions are shown in Supplementary Figure 2.A.

Computational modeling (cognitive models). In this section, we first present the perceptual learning model of family *fam*$_L$. We secondly provide the expression of the related trialwise PWPEs, followed by a description of how these errors vary with the size of the temporal integration window that we introduced. Details about MMN simulations are then provided. Finally, we describe the data for model inversion (single-trial cortical activity reconstructed using fused EEG-MEG source inversion), as well as the inversion procedure.

- Learning models

Learning models in *fam*$_L$ assume that the brain learns from each stimulus exposure the probability μ to have a deviant, in order to predict the next sound category u (with $u = 1$ in the case of a deviant and $u = 0$ in the case of a standard). We define $u \sim \mathcal{B}ern\ (\mu)$ with $\mathcal{B}ern$ the Bernoulli distribution, and $\mu \sim \mathcal{B}eta\ (\alpha, \beta)$ with α and β the parameters of the distribution $\mathcal{B}eta$, corresponding in the current case to deviant and standard counts, respectively. At trial k, we have:

$$\begin{cases} p(u_k|\mu_{k-1}) = {\mu_{k-1}}^{u_k}(1-\mu_{k-1})^{1-u_k} \\ p(\mu_k|u_k) = \dfrac{p(u_k|\mu_{k-1})p(\mu_{k-1})}{p(u_k)} \end{cases} \tag{2}$$

The posterior distribution of μ is in the form of a $\mathcal{B}eta$ distribution ($\mathcal{B}eta$ distribution is conjugate to the $\mathcal{B}ern$ distribution), leading to the following updated expression of μ at trial k:

$$\mu_k = \frac{\Gamma(\alpha_k)\Gamma(\beta_k)}{\Gamma(\alpha_k + \beta_k)} \tag{3}$$

With Γ the Gamma Euler function, and α and β following update equations:

$$\begin{cases} \alpha_k = u_k + \alpha_{k-1} \\ \beta_k = 1 - u_k + \beta_{k-1} \end{cases} \tag{4}$$

PWPE in fam_L is the Kullback-Leibler (KL) divergence between the prior and the posterior $\mathcal{B}eta$ distributions of μ, also referred to as a Bayesian Surprise (BS) in the MMN study by Ostwald et al. [23]. At trial k, it expresses as:

$$\begin{aligned} &BS(u_k) \\ &= \log\left(\frac{\Gamma(\alpha_{k-1}+\beta_{k-1})}{\Gamma(\alpha_k+\beta_k)}\right) + \log\left(\frac{\Gamma(\alpha_k)}{\Gamma(\alpha_{k-1})}\right) \\ &+ \log\left(\frac{\Gamma(\beta_k)}{\Gamma(\beta_{k-1})}\right) + (\alpha_{k-1}-\alpha_k)[\psi(\alpha_{k-1}) - \psi(\alpha_{k-1}+\beta_{k-1})] \\ &+(\beta_{k-1}-\beta_k)\,[\psi(\beta_{k-1}) - \psi(\alpha_{k-1}+\beta_{k-1})\,] \end{aligned} \tag{5}$$

With ψ the digamma Euler function.

- Variation of BS with the size of the temporal integration window

The size of the temporal integration window was parameterized by τ which enters standard and deviant count updates as follows:

$$\begin{cases} \alpha_k = u + e^{-\frac{1}{\tau}}\alpha_{k-1} \\ \beta_k = (1-u) + e^{-\frac{1}{\tau}}\beta_{k-1} \end{cases} \tag{6}$$

From equation Eq. 5 we see that the larger the τ, the larger the weight applying to past observations, leading to a more informed learning (an illustration can be found in Figure 4.C). This leads to lower BS as can be seen in Supplementary Figure 1.

- Simulations of group-level MMN

For each subject, we simulated individual trial-by-trial PWPE trajectories induced by UC and PC sequences for τ in $\{6,8,10,12,14,16,18,20,25,30,40,50,75,100\}$, using VBA [34]. We then selected PWPE values obtained for each standard preceding a deviant and for each deviant (in keeping with sensor-level trial rejection). Using exactly the

same procedure that had been used to compute the event-related difference response at the sensor level, we could simulate the group-average MMN amplitude in conditions UC and PC (arbitrary units). Results are provided in Figure 4.A.

- Trial-wise reconstructed cortical data

Model predictions were confronted to trial-by-trial timeseries collected with EEG and MEG. Single-trial data was obtained in a preparatory step involving the distributed source reconstruction of EEG-MEG data. Advanced methods were employed for source inversion with realistic forward models for both modalities[64], Bayesian framework enabling Multiple Sparse Priors [65,66], EEG-MEG fusion [67], and group-level inference [68]. Source inversions were all performed with the SPM software (SPM8 release). First, in a prior study [33] six cortical clusters could be identified from the inversions of early and late (MMN) mismatch peaks. These sources were located in the left and right Heschl's Gyrus (lHG and rHG, respectively), Planum Polare (lPP and rPP) and Inferior Frontal Gyrus (lIFG and rIFG) (see Figure 2.A). Critically, they subsequently served as spatial priors to constrain the distributed inversion of entire single-trial epochs (from -200 ms to +410 ms, 674 trials per condition per participant). Within each cluster and for each trial, reconstructed cluster-node activities were averaged to derive a cluster-level and single-trial trace being informed by both EEG and MEG data. As a control, we computed the grand-average difference response (using exactly the same procedure as for the sensor-level analysis and in keeping with individual bad trial rejection) for each cluster. Resulting group-level traces are presented in Supplementary Figure 2.B and exhibit the predictability effect (UC vs. PC) at the latency of the MMN (around 175 ms) for all clusters.

- Model inversion

Model inversions were performed with the VBA toolbox [34] at each time sample of trial-wise cortical timeseries. To reduce the number of inversions, we restricted the time interval to -50 ms to 350 ms and considered one every two samples, leading to 41 samples to cover the entire time-window. Family fam_L included four models with τ in $\{2,6,10,100\}$. Consequently, in the first analysis (*PL-oddball*), given the 7 models (one in fam_{Null}, two in fam_{NoL} and four in $fam_{L)}$, 6 clusters and 41 samples, 1722 inversions were carried out per subject (N=20). Individual UC and PC data (4 sessions) were processed all at once (multi-session inversions), and bad trials (with regard to sensor-level artifact rejection) were processed in a way that corresponding signals would not corrupt parameter optimization (note that related stimuli still entered learning dynamics because they were observed by the brain). Regarding model specifications in VBA, we assumed a deterministic evolution model (no state noise was introduced in the evolution model) and used VBA defaults priors for the measurement noise. Initial states values (involved in fam_{NoL} and fam_L) and prior distributions of learning quantities across models are given in Supplementary Table 1. Model inversions in *PL-oddball* analysis provided in particular posterior estimates of observation parameters θ_1,ε_1, ε_2 defined in Equation Eq.1 and the free energy at convergence approximating posterior model evidence. In the subsequent *PL-predictability* analysis, model space was restricted to one model, corresponding to fam_L augmented with an evolution parameter to be estimated (parameter τ). Temporal samples included in this analysis were those exhibiting fam_L as the winning family in the *PL-oddball* analysis (the number of samples consequently varied across sources, leading to a total of 33 samples). Condition UC and PC were treated separately and multi-session inversion was employed within each condition to fit the two acquisition sessions per condition at once. Overall, 66 inversions were conducted per subject (1 model, 2 conditions, 33 samples). Other model

specifications were identical to those of *PL-oddball* analysis (described above).

Neural modeling (Dynamic Causal Modeling, DCM). We start by describing the cortical sources considered throughout the different DCM analyses reported in the study. We then present two model spaces specifically designed to address the structure and the connectivity of the DCM for passive oddball sequence processing. Following subsections address EEG and MEG evoked responses entering model inversions, and model inversion specification. We finally describe the procedure developed here to combine EEG and MEG DCMs. A general description of DCM and the canonical micro-circuitry (CMC) is illustrated in Supplementary Figure 3.

- DCM sources

DCM architecture involved the sources of the early and late (MMN) components that we previously reconstructed using fused EEG-MEG inversion [33] with the current standard (preceding a deviant) and deviant evoked responses. In addition to the 6 bilateral clusters identified over Heschl's Gyrus (HG), the Planum Polare (PP), and the Inferior Frontal Gyrus (IFG), we assumed a bilateral superior frontal contribution (SF). SF clusters resulted from the fused source reconstruction of the difference between UC and PC deviance responses over the significant time intervals reported in Lecaignard et al. [30], spanning the early predictability effect and the MMN. Left and right frontal clusters (36 and 29 nodes respectively, thresholded at $p < 0.05$ with Family Wise Error (FWE) whole-brain correction) were found for the early effect, and a left contribution of 34 nodes for the MMN interval (with $p < 0.001$ not corrected). Importantly, along the study, we took into consideration the weak spatial reliability of these sources, that were however found necessary to account for the dynamics of standard and deviant evoked responses. Each of the 8 resulting clusters led to an

equivalent current dipole (ECD) located at the averaged position of local maxima over the different time intervals. MNI coordinates are provided in Figure 3.A.

- The *Network-Structure* model space

This model space is dedicated to the *DCM-oddball* analysis, to test the architecture and the inputs of DCM. It is partitioned over five architecture families (*A1*, *A2*, *A3*, *A4* and *A5)* and two input families (*HG* and *HG-IFG*), depicted in Supplementary Figure 4. Here, we assumed forward and backward trial-specific modulations (TSM), as already reported in several MMN-DCM studies [38]. For TSM applying on the self-inhibition connection strength of the superficial pyramidal cells (subpopulation SP), also referred to as the intrinsic modulation, we integrated over the two possible hypotheses (presence or absence of modulation). DCM with CMC also includes extrinsic *modulatory* connections to enable the top-down indexation of subpopulation SP excitability on the output activity of higher-level feedbacking sources. Like for the intrinsic modulation, model space was made to integrate over the two alternative hypotheses (presence or absence of modulatory connections). The resulting model space thus embedded 36 models (Supplementary Figure 4).

- The *Coupling-Change* model space

The *Coupling-Change* model space was dedicated to address precisely the effective (directed) connectivity at play during passive listening within the winning DCM network (architecture *A5* and double-input *HG-IFG*). We addressed in particular TSM applying on forward, backward, and intrinsic connections. For forward and intrinsic TSMs, two model families were considered each, corresponding to TSM enabled at all or none connections. Regarding backward TSMs, their effect depends on the above-mentioned extrinsic modulatory connections, if any. Specifically, they apply to backward extrinsic

connections in the absence of modulatory connections, and to intrinsic connections otherwise [17]. This led us to consider three model families corresponding to backward TSM i) disabled, ii) enabled without and iii) enabled with modulatory connections. A total of 14 models composed this model space.

- Data for model inversion: EEG and MEG evoked responses

EEG and MEG averaged responses evoked by standards just preceding a deviant and by deviants were considered for all DCM analyses presented in the current study. EEG responses were re-referenced to the averaged mastoid electrodes. Time interval of 0 ms to 220 ms after sound onset was used for model inversion. It was defined from sensor-level (EEG and MEG) statistical analysis on deviance responses to ensure it encompasses the MMN (and no later components). A Hanning window was applied to time-series to ensure that system's dynamics was set to zero before being excited. Data reduction achieved within the inversion procedure led to the selection of 8 (±2.7) and 13 spatial modes with EEG and MEG data, respectively (on average across subjects).

- Model inversion

DCM analyses were performed with SPM12 (Wellcome Department of Imaging Neuroscience, http://www.fil.ion.ucl.ac.ik/spm). We used the canonical micro-circuit (CMC) neural mass model [17,48] to exploit its relevance to test predictive coding predictions. We used default values of SPM12 as prior expectations and prior variance for each DCM parameter to be estimated. Each DCM inversion involved standard response as the initial state of the system and deviant response resulting from the experimental perturbation. Regarding DCM sources, we maintained dipole locations

fixed (but not their orientation) to inform spatially DCM inversion with the group-level MEG-EEG information. For each modality (EEG, MEG), the forward model used for DCM inversion was an advanced realistic Boundary Element Model (BEM) computed with Openmeeg software [64].

- Fusion of EEG and MEG DCMs

To date, the fusion of EEG and MEG data within the generative model of DCM is not implemented. Our approach consisted in performing EEG and MEG DCM inversions separately (using exactly the same parameter priors), and in a second step, exploiting the Bayesian framework of DCM to derive posterior estimates informed by both modalities (referred to as p-MEEG). Precisely, the proposed procedure rests on the assumption of conditional independence of EEG and MEG data under the quasi-static approximation of Maxwell equations, which is largely admitted for signals below 1kHz (as is the case here). Denoting EEG and MEG data by y_{EEG} and y_{MEG}, respectively, we have:

$$p(y_{EEG}, y_{MEG}) = p(y_{EEG})p(y_{MEG}) \tag{7}$$

And posterior model evidence of model m can be approximated using unimodal EEG and MEG model evidences:

$$p(y_{EEG}, y_{MEG}|m) = p(y_{EEG}|m)p(y_{MEG}|m) \tag{8}$$

Consequently, $\mathcal{F}_{p-MEEG}$ the variational free energy approximation to p-MEEG model log-evidence could be obtained by:

$$\mathcal{F}_{p-MEEG}(m) \approx \mathcal{F}_{EEG}(m) + \mathcal{F}_{MEG}(m) \tag{9}$$

With $\mathcal{F}_{EEG}$ and $\mathcal{F}_{MEG}$ the free energy values for EEG and MEG respectively. Besides, the posterior distribution of some DCM parameter θ under model m writes given:

$$p(\theta|y_{EEG}, y_{MEG}) = \frac{p(y_{EEG}, y_{MEG}|\theta)p(\theta)}{p(y_{EEG}, y_{MEG})} \tag{10}$$

Which can be re-formulated as follows to reveal the posterior distributions of θ deriving from unimodal inversion of EEG and MEG data:

$$p(\theta|y_{EEG}, y_{MEG}) = \frac{p(\theta|y_{EEG})p(\theta|y_{MEG})}{p(\theta)} \tag{11}$$

DCM approach assumes every parameter θ to have of the form of a Gaussian distribution. Hence prior distribution expresses as $q(\theta) \sim \mathcal{N}(\mu_o, \sigma_o)$. We also denote $q(\theta, y_{EEG}) \sim \mathcal{N}(\mu_e, \sigma_e)$, $q(\theta, y_{MEG}) \sim \mathcal{N}(\mu_m, \sigma_m)$ and $q(\theta, y_{EEG}, y_{MEG}) \sim \mathcal{N}(\mu_p, \sigma_p)$ the posterior distribution of θ given EEG data, MEG data and EEG-and-MEG data respectively. We have μ_{em} and σ_{em} the mean and variance of the distribution resulting from the multiplication of $q(\theta, y_{EEG})$ and $q(\theta, y_{MEG})$. From equation Eq.10 and the analytical expressions of μ_{em} and σ_{em} (detailed in most statistic books), we derive:

$$\begin{cases} \sigma_p = \dfrac{\sigma_o \sigma_{em}}{\sigma_o - \sigma_{em}} \\ \mu_p = \mu_{em} + \dfrac{(\mu_{em} - \mu_o)\sigma_p}{\sigma_o} \end{cases} \tag{12}$$

Statistical analysis.

PL-oddball analysis. We ran a family-level comparison [35] with a Random Effects (RFX) model at each cluster and each time sample. Each comparison provided the posterior exceedance probability of each family (fam_{null}, fam_{NoL}, fam_{L}) that quantifies in a statistically principled way how the related family is likely to outperform others.

PL-predictability analysis. We assumed a constant value of τ within the time interval used for model inversion (spanning the MMN). We therefore averaged τ estimates across samples for each cluster. Predictability effect could thus be analyzed by conducting a repeated-measures ANOVA on these posterior estimates with factors *Condition* (UC, PC), *Hemisphere* (Left, Right) and *Sources* (HG, PP, IFG).

DCM-oddball analysis. The first analysis involves the *Network-Structure* model space with data in condition UC and PC. For each condition, DCMs obtained in each modality (EEG, MEG) were fused using the above-described approach. We then combined p-MEEG DCMs across conditions (UC, PC) using similar Bayesian reasoning (log-posterior model evidences were summed across conditions). We then quantitatively evaluated the architecture and the input families using family-level inference (Penny et al., 2010) with an RFX model, based on the p-MEEG approximations of model evidence ($\mathcal{F}_{p-MEEG}$). The second analysis involves the *Coupling-Change* model space and rests on p-MEEG DCMs in conditions UC and PC. Family level inference (RFX model) combined both conditions, and was conducted over the forward, backward and intrinsic TSM factor. As each of these three family comparisons indicated standard-to-deviant changes, we subsequently examined TSM estimates in each condition separately to determine the direction of change (a value larger than one would indicate larger connection strength in deviants than in standards, and *vice-versa*). For each

condition, we used Bayesian model averaging (BMA) to derive group-level posterior estimates averaged across model space (with model-evidence weighting) and across subjects. Each estimate was informed by EEG and MEG using equation Eq.11. For each connection type, BMA estimates were averaged over the entire network.

DCM-predictability analysis. To test the predictability effect on DCM connectivity, we compared individual BMA posterior estimates (in the p-MEEG modality) across conditions, and computed over the *Coupling-Change* model space. The analysis rests on four connections in particular: forward and self-inhibition connection strengths (indicated by a black star in Supplementary Figure 3, right), and their respective forward and intrinsic TSM. Note that DCM with CMC assumes two types of forward connections: a predominant one originating in superficial pyramidal (SP) subpopulation and targeting the spiny stellate (SS) cells of the higher-level source, and a secondary one linking subpopulation SP to higher-level deep pyramidal (DP) subpopulation (Supplementary Figure 3, left). Here, we report only the effect of predictability on the former type. For each of the four parameters, we conducted a repeated-measures ANOVA over individual BMA estimates with factors *Condition* (UC, PC), *Hemisphere* (Left, Right) and *Level* (HG-PP, PP-IFG, IFG-SF); in the case of self-inhibition parameter and intrinsic TSM, this latter factor was replaced by factor *Source* (HG, PP, IFG, SF).

Throughout the paper, ANOVA analyses were performed using R software (The R Foundation, https://www.r-project.org/).

Acknowledgments

We thank Sébastien Daligault and Pascal Calvat for programming support in interfacing with the CC IN2P3. We acknowledge CC-IN2P3 for providing computing resources and services needed for this work. We thank Emmanuel Maby and Gaëtan Sanchez for helpful discussions. This work was supported by a grant from the Agence Nationale de la Recherche of the French Ministry of Research ANR-11-BSH2-001-01 to AC and FL and a grant from the Fondation pour la Recherche Médicale (FRM) to OB and JM. This work was conducted in the framework of the LabEx CeLyA ("Centre Lyonnais d'Acoustique", ANR-10-LABX-0060) and of the LabEx Cortex ("Construction, Function and Cognitive Function and Rehabilitation of the Cortex", ANR-10-LABX-0042) of Université de Lyon, within the program "Investissements d'avenir" (ANR-11-IDEX-0007) operated by the French National Research Agency (ANR).

Author Contributions

Conceptualization, AC, FL and JM; Methodology, FL and JM; Software, FL and JM; Investigation, AC and FL; Writing, AC, FL and JM; Funding Acquisition, OB, AC and JM; Supervision, OB, AC and JM.

Declaration of Interest

The authors declare that they have no conflict of interests.

Supplemental Figures and Table

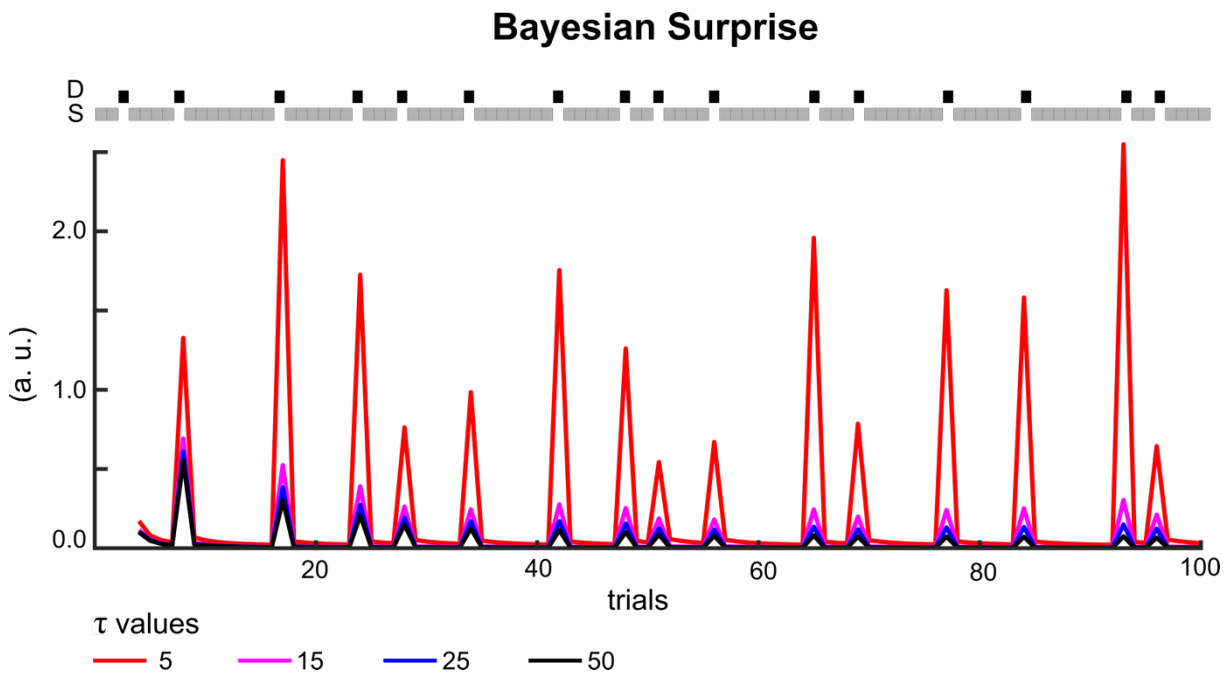

Figure 1. Bayesian surprise as a function of τ. (*arbitrary units, a. u.) Illustration of different BS trajectories obtained with varying τ, for the first 100 stimuli of a typical UC oddball sequence. Two comments should be made: 1) BS decreases as τ increases and 2) whatever τ, BS is larger for deviants (D, black squares) than for standards (S, grey squares).*

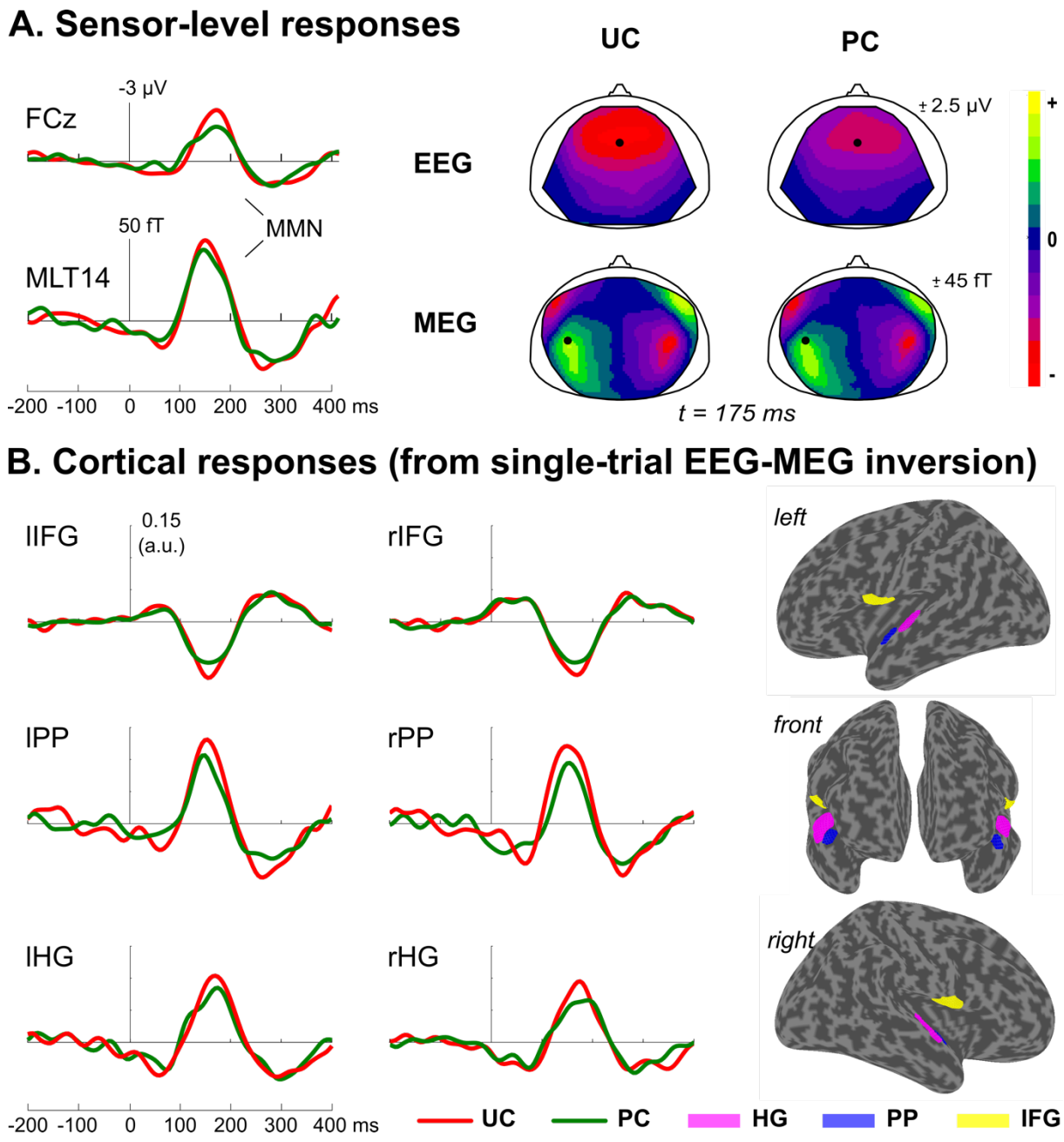

Figure 2. Mismatch responses for model inversion (2-20 Hz). *A) Group-average difference responses measured with EEG (upper row, 63 electrodes, averaged-mastoid reference) and MEG (lower row, 275 gradiometers). Left: a typical MMN is indicated around 175 ms, as illustrated at electrode FCz and gradiometer MLT14, in both contexts (UC: red, PC: green). Right: corresponding group-level sensor-level maps at 175 ms. Black dots refer to FCz (EEG maps, upper row) and MLT14 (MEG maps, lower row). B) Reconstructed mismatch response in condition UC and PC (red,*

green, resp.) obtained at the group-level from the individual EEG-MEG source reconstruction of single-trial traces, at six clusters engaged in MMN processing. Cluster labeling is provided in the main text. These bilateral clusters are described (right panels) on the inflated template cortex (SPM) using left, front, and right views, color code for clusters at the bottom right.

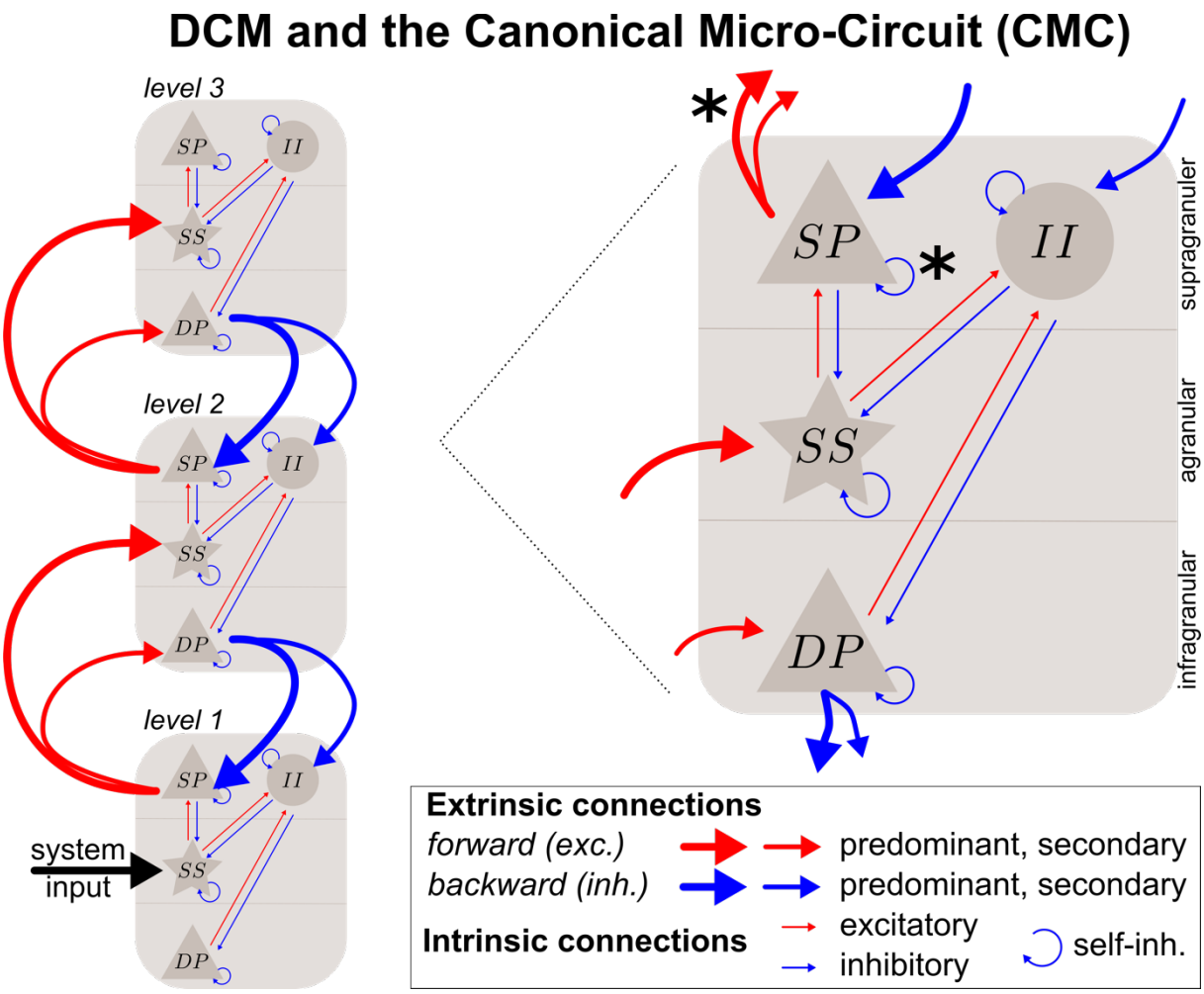

Figure 3. Schematic description of DCM with the Canonical Micro-Circuit [26]*. Left, example of a three-level DCM with sensory input (black arrow) targeting the lower level. Color and strength of connections indicate their category, as indicated in the legend. Right, detailed view of a DCM source (level), embedding a canonical micro-circuitry. It*

comprises three layers (infragranular, agranular and supragranular) and involves four cell suppopulations (DP: deep pyramidal; SS: spiny stellate; SP: superior pyramidal; II: inhibitory interneurons). Black stars indicate the predominant forward and self-inhibitory connections that were examined in the DCM-predictability analysis, because they could represent PE (or PWPE) and PW, respectively, according to predictive brain models. Trial-specific modulations (TSM) reflecting standard-to-deviant changes are not represented. Forward and backward TSM apply on forward and backward extrinsic connections, respectively, and intrinsic TSM applies on self-inhibition in SP. exc.: excitatory; inh.: inhibitory.

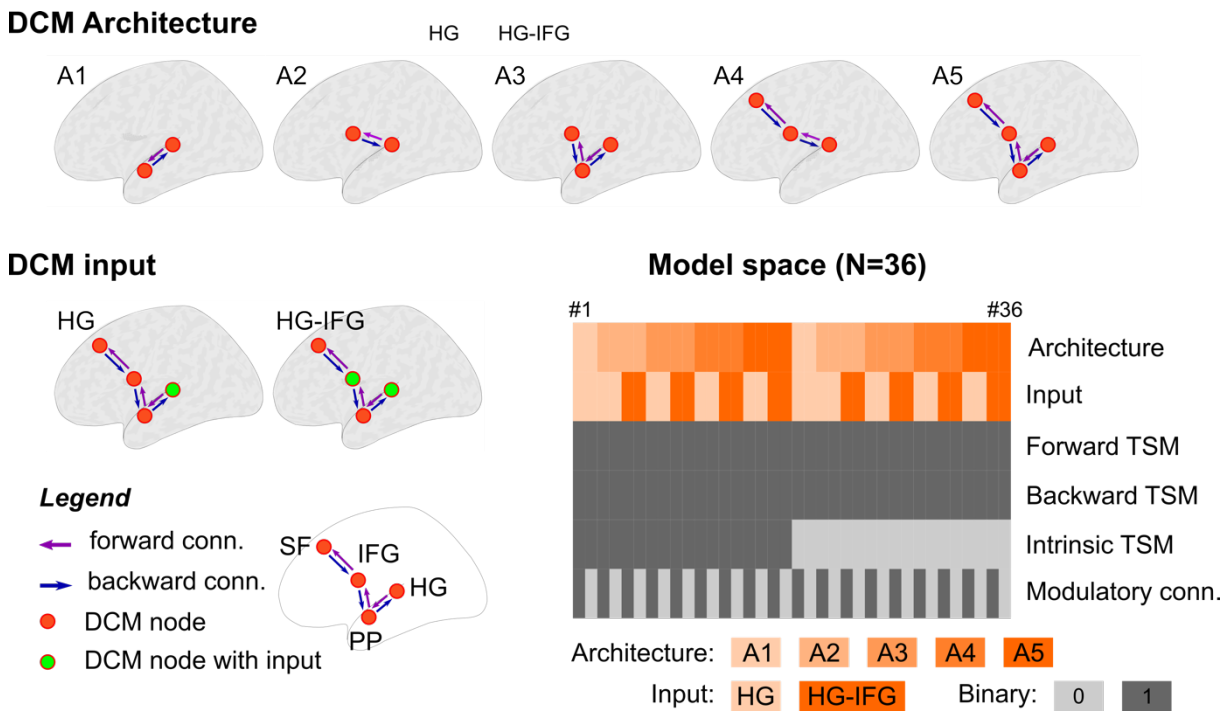

Figure 4. Network-Structure model space. *Upper row, schematic view of the five model families designed to test DCM architecture in deviance processing. Bottom left,*

the two model families of DCM input, HG and HG-IFG. Color codes of extrinsic connections (conn.) and DCM source (or node) are provided in the legend. Source labels HG, PP, IFG and SF: Heschl's Gyrus, Planum Polare, Inferior Frontal Gyrus and Superior Frontal. Bottom Right Table: DCM specifications for each of the 36 models (in columns). TSM: Trial-Specific Modulations accounting for standard-to-deviant changes in connectivity. Frontal, Backward and Intrinsic TSM, as well as Modulatory connections correspond to binary options (enabled = 1, disabled= 0) applying to the entire network.

		Initial state values		Ev. Par		Obs. Par	
family	*model*						
fam_{null}	null	-	-	-	-	θ_2	$(0, 100)$
fam_{noL}	CD	previous observation	$(0, 0)$	-	-	θ_1	$(0, 100)$
						θ_2	$(0, 100)$
	LinCD	previous observation	$(0, 0)$	-	-	θ_1	$(0, 100)$
		observed standards	$(0, 0)$	-	-	θ_2	$(0, 100)$
fam_L	fixed τ	standard count	$(1, 0)$	-	-	θ_1	$(0, 100)$
		deviant count	$(1, 0)$	-	-	θ_2	$(0, 100)$
	free τ	standard count	$(1, 0)$	τ	$(\log(10), 10)$	θ_1	$(0, 100)$
		deviant count	$(1, 0)$			θ_2	$(0, 100)$

Table 1. Sufficient statistics (mean, variance) for initial conditions and model parameters. *Ev. Par.: Evolution parameters; Obs. Par.: Observation parameters. For family fam_{noL}, previous observation set to 0 correspond to a standard sound. θ_1 and θ_2 refers to Equation Eq.1. Initial states values were not estimated during model inversion (variance is set to 0).*

References

1. Dayan, P., Hinton, G. E., Neal, R. M. & Zemel, R. S. The Helmholtz machine. *Neural Comput* **7,** 889–904 (1995).
2. Friston, K. The history of the future of the Bayesian brain. *NeuroImage* **62,** 1230–1233 (2012).
3. Mathys, C. D. *et al.* Uncertainty in perception and the Hierarchical Gaussian Filter. *Front Hum Neurosci* **8,** 825 (2014).
4. Friston, K. The free-energy principle: a unified brain theory? *Nat Rev Neurosci* **11,** 127–138 (2010).
5. Clark, A. Whatever next? Predictive brains, situated agents, and the future of cognitive science. *Behav Brain Sci* **36,** 181–204 (2013).
6. Behrens, T. E. J., Woolrich, M. W., Walton, M. E. & Rushworth, M. F. S. Learning the value of information in an uncertain world. *Nat Neurosci* **10,** 1214–1221 (2007).
7. Tenenbaum, J. B., Kemp, C., Griffiths, T. L. & Goodman, N. D. How to grow a mind: statistics, structure, and abstraction. *Science* **331,** 1279–1285 (2011).
8. Vossel, S. *et al.* Spatial attention, precision, and Bayesian inference: a study of saccadic response speed. *Cereb Cortex* **24,** 1436–1450 (2014).
9. Dehaene, S., Meyniel, F., Wacongne, C., Wang, L. & Pallier, C. The Neural Representation of Sequences: From Transition Probabilities to Algebraic Patterns and Linguistic Trees. *Neuron* **88,** 2–19 (2015).
10. Auksztulewicz, R. & Friston, K. Attentional Enhancement of Auditory Mismatch Responses: a DCM/MEG Study. *Cerebral Cortex* (2015). doi:10.1093/cercor/bhu323
11. Schröger, E., Marzecová, A. & Sanmiguel, I. Attention and prediction in human audition: a lesson from cognitive psychophysiology. *Eur J Neurosci* **41,** 641–664 (2015).
12. Heilbron, M. & Chait, M. Great Expectations: Is there Evidence for Predictive Coding in Auditory Cortex? *Neuroscience* **389,** 54–73 (2018).
13. Lumaca, M., Trusbak Haumann, N., Brattico, E., Grube, M. & Vuust, P. Weighting of neural prediction error by rhythmic complexity: A predictive coding account using mismatch negativity. *Eur J Neurosci* (2018). doi:10.1111/ejn.14329
14. Friston, K. & Kiebel, S. Predictive coding under the free-energy principle. *Journal of Mathematical Psychology* **364,** 1211–1221 (2009).
15. Kok, P. & de Lange, F. P. in *An Introduction to Model-Based Cognitive Neuroscience* (eds. Wagenmakers, E.-J. & Forstmann, B. U.) 221–244 (2015).
16. Markov, N. T. & Kennedy, H. The importance of being hierarchical. *Curr Opin Neurobiol* **23,** 187–194 (2013).
17. Bastos, A. M. *et al.* Canonical microcircuits for predictive coding. *Neuron* **76,** 695–711 (2012).
18. Mathys, C. D., Daunizeau, J., Friston, K. & Stephan, K. E. A bayesian foundation for individual learning under uncertainty. *Front Hum Neurosci* **5,** 39 (2011).
19. Adams, R. A., Stephan, K. E., Brown, H. R., Frith, C. D. & Friston, K. The computational anatomy of psychosis. *Front Psychiatry* **4,** 47 (2013).
20. Stephan, K. E., Iglesias, S., Heinzle, J. & Diaconescu, A. O. Translational Perspectives for Computational Neuroimaging. *Neuron* **87,** 716–732 (2015).
21. Lawson, R. P., Mathys, C. D. & Rees, G. Adults with autism overestimate the volatility of the sensory environment. *Nat Neurosci* **15,** 173–13 (2017).

22. Iglesias, S. *et al.* Hierarchical Prediction Errors in Midbrain and Basal Forebrain during Sensory Learning. *Neuron* **80,** 519–530 (2013).
23. Ostwald, D. *et al.* Evidence for neural encoding of Bayesian surprise in human somatosensation. *NeuroImage* **62,** 177–188 (2012).
24. Lieder, F., Daunizeau, J., Garrido, M. I., Friston, K. & Stephan, K. E. Modelling trial-by-trial changes in the mismatch negativity. *PLoS Comput Biol* **9,** 1–16 (2013).
25. Escera, C., Leung, S. & Grimm, S. Deviance detection based on regularity encoding along the auditory hierarchy: electrophysiological evidence in humans. *Brain Topogr* **27,** 527–538 (2014).
26. Friston, K. A theory of cortical responses. *Philosophical Transactions of the Royal Society B: Biological Sciences* **360,** 815–836 (2005).
27. Garrido, M. I., Kilner, J. M., Kiebel, S. & Friston, K. Dynamic causal modeling of the response to frequency deviants. *Journal of Neurophysiology* **101,** 2620–2631 (2009).
28. Moran, R. *et al.* Free energy, precision and learning: the role of cholinergic neuromodulation. *Journal of Neuroscience* **33,** 8227–8236 (2013).
29. Lopes da Silva, F. EEG and MEG: relevance to neuroscience. *Neuron* **80,** 1112–1128 (2013).
30. Lecaignard, F., Bertrand, O., Gimenez, G., Mattout, J. & Caclin, A. Implicit learning of predictable sound sequences modulates human brain responses at different levels of the auditory hierarchy. *Front Hum Neurosci* **9,** 505 (2015).
31. Marr, D. *Vision: A Computational Approach*. (1982).
32. Kiebel, S., Garrido, M. I., Moran, R., Chen, C. C. & Friston, K. Dynamic causal modeling for EEG and MEG. *Hum. Brain Mapp.* **30,** 1866–1876 (2009).
33. Lecaignard, F., Bertrand, O., Caclin, A. & Mattout, J. Empirical evaluation of fused EEG-MEG source reconstruction. Application to auditory mismatch generators. biorxiv 765966.
34. Daunizeau, J., Adam, V. & Rigoux, L. VBA: a probabilistic treatment of nonlinear models for neurobiological and behavioural data. *PLoS Comput Biol* **10,** e1003441 (2014).
35. Penny, W. D. *et al.* Comparing families of dynamic causal models. *PLoS Comput Biol* **6,** e1000709 (2010).
36. Mattout, J., Henson, R. & Friston, K. Canonical source reconstruction for MEG. *Computational Intelligence and Neuroscience* 67613 (2007). doi:10.1155/2007/67613
37. Auksztulewicz, R. & Friston, K. Repetition suppression and its contextual determinants in predictive coding. *CORTEX* (2016). doi:10.1016/j.cortex.2015.11.024
38. Garrido, M. I., Kilner, J. M., Stephan, K. E. & Friston, K. The mismatch negativity: a review of underlying mechanisms. *Clin Neurophysiol* **120,** 453–463 (2009).
39. Phillips, H. N., Blenkmann, A., Hughes, L. E., Bekinschtein, T. A. & Rowe, J. B. Hierarchical Organization of Frontotemporal Networks for the Prediction of Stimuli across Multiple Dimensions. *Journal of Neuroscience* **35,** 9255–9264 (2015).
40. Chennu, S. *et al.* Silent Expectations: Dynamic Causal Modeling of Cortical Prediction and Attention to Sounds That Weren't. *J Neurosci* **36,** 8305–8316 (2016).

41. Garrido, M. I., Rowe, E. G., Halasz, V. & Mattingley, J. B. Bayesian Mapping Reveals That Attention Boosts Neural Responses to Predicted and Unpredicted Stimuli. *Cereb Cortex* **28,** 1771–1782 (2018).
42. Deouell, L. Y. The Frontal Generator of the Mismatch Negativity Revisited. *Journal of Psychophysiology* **21,** 188–203 (2007).
43. Brown, H. R. & Friston, K. Dynamic causal modelling of precision and synaptic gain in visual perception - an EEG study. *NeuroImage* **63,** 223–231 (2012).
44. Feldman, H. & Friston, K. Attention, uncertainty, and free-energy. *Front Hum Neurosci* **4,** 215 (2010).
45. Southwell, R. *et al.* Is predictability salient? A study of attentional capture by auditory patterns. *Journal of Mathematical Psychology* **372,** (2017).
46. Tillmann, B., Bigand, E. & Pineau, M. Effects of Global and Local Contexts on Harmonic Expectancy. *Music Perception: An Interdisciplinary Journal* **16,** 99–117 (1998).
47. Rohenkohl, G., Cravo, A. M., Wyart, V. & Nobre, A. C. Temporal expectation improves the quality of sensory information. *Journal of Neuroscience* **32,** 8424–8428 (2012).
48. Brown, H. R. & Friston, K. The functional anatomy of attention: a DCM study. *Front Hum Neurosci* **7,** 784 (2013).
49. Auksztulewicz, R. *et al.* The Cumulative Effects of Predictability on Synaptic Gain in the Auditory Processing Stream. *Journal of Neuroscience* **37,** 6751–6760 (2017).
50. Pinotsis, D. A. *et al.* Linking canonical microcircuits and neuronal activity_ Dynamic causal modelling of laminar recordings. *NeuroImage* **146,** 355–366 (2017).
51. Phillips, H. N. *et al.* Convergent evidence for hierarchical prediction networks from human electrocorticography and magnetoencephalography. *CORTEX* **82,** 192–205 (2016).
52. Garrido, M. I., Kilner, J. M., Kiebel, S. & Friston, K. Evoked brain responses are generated by feedback loops. *Proc Natl Acad Sci USA* **104,** 20961–20966 (2007).
53. Chennu, S. *et al.* Expectation and attention in hierarchical auditory prediction. *Journal of Neuroscience* **33,** 11194–11205 (2013).
54. Dürschmid, S. *et al.* Hierarchy of prediction errors for auditory events in human temporal and frontal cortex. *Proc Natl Acad Sci USA* 201525030–6 (2016). doi:10.1073/pnas.1525030113
55. Chao, Z. C., Takaura, K., Wang, L., Fujii, N. & Dehaene, S. Large-Scale Cortical Networks for Hierarchical Prediction and Prediction Error in the Primate Brain. 1–19 (2018). doi:10.1016/j.neuron.2018.10.004
56. David, O., Maess, B., Eckstein, K. & Friederici, A. D. Dynamic Causal Modeling of Subcortical Connectivity of Language. *J Neurosci* **31,** 2712–2717 (2011).
57. Meyniel, F., Maheu, M. & Dehaene, S. Human Inferences about Sequences: A Minimal Transition Probability Model. *PLoS Comput Biol* **12,** e1005260 (2016).
58. Friston, K. Hierarchical Models in the Brain. **4,** e1000211 (2008).
59. Kanai, R., Komura, Y., Shipp, S. & Friston, K. Cerebral hierarchies: predictive processing, precision and the pulvinar. *Philosophical Transactions of the Royal Society B: Biological Sciences* **370,** 20140169–20140169 (2015).
60. Meyniel, F. & Dehaene, S. Brain networks for confidence weighting and hierarchical inference during probabilistic learning. *Proc Natl Acad Sci USA* **114,** E3859–E3868 (2017).
61. Parr, T. & Friston, K. Attention or salience? *Curr Opin Psychol* **29,** 1–5 (2018).

62. Escera, C., Alho, K., Schröger, E. & Winkler, I. Involuntary attention and distractibility as evaluated with event-related brain potentials. *Audiol. Neurootol.* **5,** 151–166 (2000).
63. Aguera, P.-E., Jerbi, K., Caclin, A. & Bertrand, O. ELAN: A Software Package for Analysis and Visualization of MEG, EEG, and LFP Signals. *Computational Intelligence and Neuroscience* **2011,** 1–11 (2011).
64. Gramfort, A., Papadopoulo, T., Olivi, E. & Clerc, M. OpenMEEG: opensource software for quasistatic bioelectromagnetics. *Biomed Eng Online* **9,** 45 (2010).
65. Mattout, J., Phillips, C., Penny, W. D., Rugg, M. D. & Friston, K. MEG source localization under multiple constraints: an extended Bayesian framework. *NeuroImage* **30,** 753–767 (2006).
66. Friston, K. *et al.* Multiple sparse priors for the M/EEG inverse problem. *NeuroImage* **39,** 1104–1120 (2008).
67. Henson, R., Mouchlianitis, E. & Friston, K. MEG and EEG data fusion: simultaneous localisation of face-evoked responses. *NeuroImage* **47,** 581–589 (2009).
68. Litvak, V. & Friston, K. Electromagnetic source reconstruction for group studies. *NeuroImage* **42,** 1490–1498 (2008).